





EGFR signaling controls directionality of epithelial multilayer formation upon loss of cell polarity

Aiguo Tian^{1,2,*} , Xian-Feng Wang¹ , Yuting Xu¹, Virginia Morejon¹, Yi-Chun Huang¹ ,
Chidi Nwapuda¹ & Wu-Min Deng^{1,2,**} 

Abstract

Apical-basal polarity is maintained by distinct protein complexes that reside in membrane junctions, and polarity loss in monolayered epithelial cells can lead to formation of multilayers, cell extrusion, and/or malignant overgrowth. Yet, how polarity loss cooperates with intrinsic signals to control directional invasion toward neighboring epithelial cells remains elusive. Using the *Drosophila* ovarian follicular epithelium as a model, we found that posterior follicle cells with loss of *lethal giant larvae (lg)* or *Discs large (Dlg)* accumulate apically toward germline cells, whereas cells with loss of *Bazooka (Baz)* or *atypical protein kinase C (aPKC)* expand toward the basal side of wildtype neighbors. Further studies revealed that these distinct multilayering patterns in the follicular epithelium were determined by epidermal growth factor receptor (EGFR) signaling and its downstream target Pointed, a zinc-finger transcription factor. Additionally, we identified *Rho kinase* as a Pointed target that regulates formation of distinct multilayering patterns. These findings provide insight into how cell polarity genes and receptor tyrosine kinase signaling interact to govern epithelial cell organization and directional growth that contribute to epithelial tumor formation.

Keywords cell polarity; *Drosophila*; EGFR signaling; follicular epithelium; growth directions

Subject Categories Cancer; Cell Adhesion, Polarity & Cytoskeleton; Development

DOI 10.15252/embj.2023113856 | Received 22 February 2023 | Revised 18 October 2023 | Accepted 20 October 2023 | Published online 13 November 2023

The EMBO Journal (2023) 42: e113856

Introduction

Epithelial cells, which form continuous sheets to provide protective, absorptive, and secretory functions, are polarized and characterized by cell membranes with apical and basolateral domains separated by adherens and tight junctions. These different domains are

defined by specific protein complexes, including the Scribble (Scrib) complex located at the septate junctions and regulates basolateral membrane identity, the Par and the Crumbs complexes that are localized at the tight junctions to regulate apical membrane identity (Bilder *et al*, 2000, 2003; Hong *et al*, 2001; Zulueta-Coarasa & Rosenblatt, 2021). The genes coding for these protein complexes (namely, polarity genes) are conserved across metazoans and they are the gatekeeper to prevent malignant growth, and disruption of their function has major implications in development and tumorigenesis (Coradini *et al*, 2011; Royer & Lu, 2011).

The behavior of polarity-deficient epithelial cells can be affected by locally available signals. In the hinge area of *Drosophila* wing imaginal discs, loss of *lethal (2) giant larvae (lg)* or *Scrib* leads to apical delamination and tumor formation, and the process requires local Jak–STAT signaling (Slattum & Rosenblatt, 2014; Tamori *et al*, 2016; Richardson & Portela, 2018; Nanavati *et al*, 2020). Similarly, in the follicular epithelium (FE) during oogenesis, the polarity-deficient follicle cells form multilayers primarily at the terminal regions of the egg chambers (Abdelilah-Seyfried *et al*, 2003; Bilder, 2004; Chatterjee *et al*, 2022). The polarity-disrupted follicle cells invade into the germline region (Goode & Perrimon, 1997; Abdelilah-Seyfried *et al*, 2003; Bilder, 2004; Chatterjee *et al*, 2022), and the intensity of invasion is enhanced by Keap1–Nrf2 signaling (Chatterjee *et al*, 2022). These findings indicate a significant contribution of tissue microenvironment in malignant transformation of polarity-loss epithelial cells.

The FE in *Drosophila* is maintained by a population of follicle stem cells located in the germarium. The descendant follicle cells experience a series of signaling events that pattern them along the axis of the egg chamber and control their differentiation and maturation. The signaling events include the Jak–STAT signaling regulated development of the polar cells, Notch-induced transition from mitotic to endocycle, and EGFR signaling-induced posterior follicle cell fate (Gonzalez-Reyes *et al*, 1995; Roth *et al*, 1995; Deng *et al*, 2001; Lopez-Schier & St Johnston, 2001; Bastock & St Johnston, 2008; Antel & Inaba, 2020). EGFR signaling is activated by interaction between the TGF- α -like ligand Gurken (Grk) in the oocyte and the epidermal growth factor receptor (EGFR, also called Torpedo) in the abutting follicle cells. When the cell polarity genes

1 Department of Biochemistry and Molecular Biology, Tulane University School of Medicine, Louisiana Cancer Research Center, New Orleans, LA, USA

2 Tulane Aging Center, Tulane University School of Medicine, New Orleans, LA, USA

*Corresponding author. Tel: +504 988 5315; E-mail: atian@tulane.edu

**Corresponding author. Tel: +504 988 5289; E-mail: wdeng7@tulane.edu

are mutated in the FE, the terminal regions of egg chambers produce the multilayering phenotype (Abdelilah-Seyfried *et al.*, 2003; Li *et al.*, 2011; Shahab *et al.*, 2015; Jevitt *et al.*, 2021), which appears to be more prominent in the posterior follicle cells (PFCs) (Shahab *et al.*, 2015).

In this study, we found that PFCs with loss of the polarity genes *lgl* or *Dlg* accumulate toward the apical side of their wildtype neighbors, whereas loss of *Baz* or *aPKC* caused basal expansion of mutant cells. The direction of accumulation or expansion is dependent on the levels of EGFR signaling. Further studies with single-cell RNA sequencing (scRNA-seq) and genetic epistasis analyses revealed that EGFR signaling determines formation of distinct multilayering patterns through the Pnt-Rok-Sqh regulatory axis. In summary, we show that cell polarity acts as a gatekeeper to prevent epithelial cells from invading their neighbors and that the tissue microenvironment regulates the growth direction of the polarity-deficient cells.

Results

Distinct multilayering patterns caused by loss of apical-basal polarity in follicle cells

The FE is a monolayered epithelium that shows a characteristic apical-basal polarity (referred to as cell polarity hereafter) with its apical surface facing the germline cells (Fig 1A–A''' and E–E'''). When follicle cell (FC) clones mutant for *lgl* (*lgl^d*) were generated using the FLP/FRT technique (Xu & Rubin, 1993), multilayers were formed at the terminal areas of egg chambers (Appendix Fig S1; 100%, $n = 90$), as reported previously (Abdelilah-Seyfried *et al.*, 2003; Li *et al.*, 2011; Shahab *et al.*, 2015; Jevitt *et al.*, 2021). Focusing on egg chambers during mid-oogenesis (stage 7–10), we noticed that the multilayers contained both mutant *lgl* and wildtype cells (Fig 1B–C'''). In the majority of posterior follicle cell (PFC) clones carrying multilayers (92.1%, $n = 63$, Fig 1D), *lgl* mutant cells were located at the apical side (Fig 1B–B''', GFP[−], red arrows) relative to their neighboring wildtype FCs (Fig 1B–B''', GFP⁺, green arrows), and these adjacent wildtype FCs were insulated from the oocyte by apically located mutant cells. In only a small fraction of clones with the multilayers (7.9%, $n = 63$, Fig 1D), *lgl* mutant cells (Fig 1C–C''', GFP[−], red arrows) were located at the basal side of their wildtype neighbors (Fig 1C–C''', GFP⁺, green arrows). To

further observe the connection between apically located mutant cells and wildtype neighbors, we performed the Z-stack analysis and marked the cytoskeleton with fluorescent Phalloidin. The mutant cells of *lgl* were apically located (Fig EV1A and A', GFP[−], red arrows, Movie EV1) and showed clear connection with wildtype neighbors (Fig EV1B–C', green arrows). These findings suggest that *lgl* mutant cells tend to be apically accumulated within the multilayers containing both mutant and wildtype cells.

The apical accumulation pattern suggests that *lgl* mutant cells could expand apically in the area between the wildtype neighbors and the oocyte. To corroborate this, we closely examined egg chambers bearing small *lgl^d* PFC clones for the relative position between mutant cells and neighboring wildtype cells at the clone boundary. In the majority of these mosaic FE (93.1%, $n = 77$, Fig 1H and F–F''' compared with Fig 1G–G'''), *lgl^d* mutant cells were found to be apically located at the interface (Fig 1F–F''', GFP[−], red arrows) and separated their wildtype neighbors from the oocyte (Fig 1F–F''', GFP⁺, green arrows). Their relative positions at the interface indicate that *lgl* mutant cells show a preferential apical accumulation to form multilayers at the apical side of adjacent wildtype cells in the FE.

The analysis of a distinct mutant allele *lgl^{27S3}* validated apical location of *lgl* mutant cells in mosaic FE containing both large (Fig EV2A, 91.4%, $n = 70$) and small clones (Fig EV2B, 92.5%, $n = 80$). To determine whether the preferential apical accumulation is specific to *lgl* mutant cells, we examined mosaic egg chambers containing PFC clones of *Dlg*, which belongs to the same Scrib complex as *Lgl*, and found that mutant cells of two *Dlg* alleles (*Dlg^{m52}* and *Dlg^{m30}*) showed similar apical accumulation in large PFC clones (Fig 2A, *Dlg^{m52}*, 93.3%, $n = 75$; Figs EV1F–F'' vs. G–G'', and EV2C, *Dlg^{m30}*, 92.3%, $n = 65$). In small clones, we noticed that *Dlg* mutant cells predominantly locate toward the apical interface of the neighboring wildtype cells (Fig 2B, *Dlg^{m52}*, 95%, $n = 81$, Fig EV1D–D'' compared with Figs EV1E–E'' and EV2D, *Dlg^{m30}*, 92.5%, $n = 65$).

During the development of egg chambers, the wildtype FCs enter the endoreplication cycle after stage 7, leading them to cease division and no longer increase in number (Deng *et al.*, 2001) (Fig 2G–G'''). In contrast, the *lgl/Dlg* mutant FCs exhibited continuous division, as indicated by expression of the mitotic cell marker PH3 (Phospho-Histone H3) (Fig 2H–H'''). This continued proliferation of *lgl/Dlg* mutant cells results in an increase in their numbers at the apical side, leading to the insulation of wildtype neighbors from the oocyte.

Figure 1. Loss of *lgl* in PFCs produces the apical location pattern.

- A–A''' Wildtype PFC clones without GFP showed the normal monolayer.
- B–B''' Mutant PFCs of *lgl^d* without GFP (red arrows) accumulated at the apical side and insulated the wildtype neighbors from the oocyte (green arrows), which generates the apical location pattern.
- C–C''' Mutant PFCs of *lgl^d* without GFP (red arrows) are localized at the basal side of the neighboring wildtype cells (green arrows) to form the basal location pattern.
- D The frequency of each location pattern was quantified (n (total clones with apical or basal location) = 63).
- E–E''' Wildtype PFC clones without GFP showed the normal monolayer.
- F–F''' At the edge of multilayers with small clones, mutant PFCs (red arrows) of *lgl^d* locate toward the apical side of their neighboring wildtype cells (green arrows).
- G–G''' At the edge of multilayers with small clones, mutant PFCs (red arrows) of *lgl^d* locate toward the basal side of their neighboring wildtype cells (green arrows).
- H The frequency of clones with apical and basal location was quantified (n (total clones with apical or basal location) = 77).

Data information: The relative location of GFP⁺ cells (green) and GFP[−] cells (red) are illustrated in A''', B''', C'', E'', F'', and G'''. a: apical side; b: basal side; O: oocyte. Phall: Phalloidin. Scale bars represent 20 μm.

Three independent experiments were performed, and error bars are ±SEM (D and H). Source data are available online for this figure.

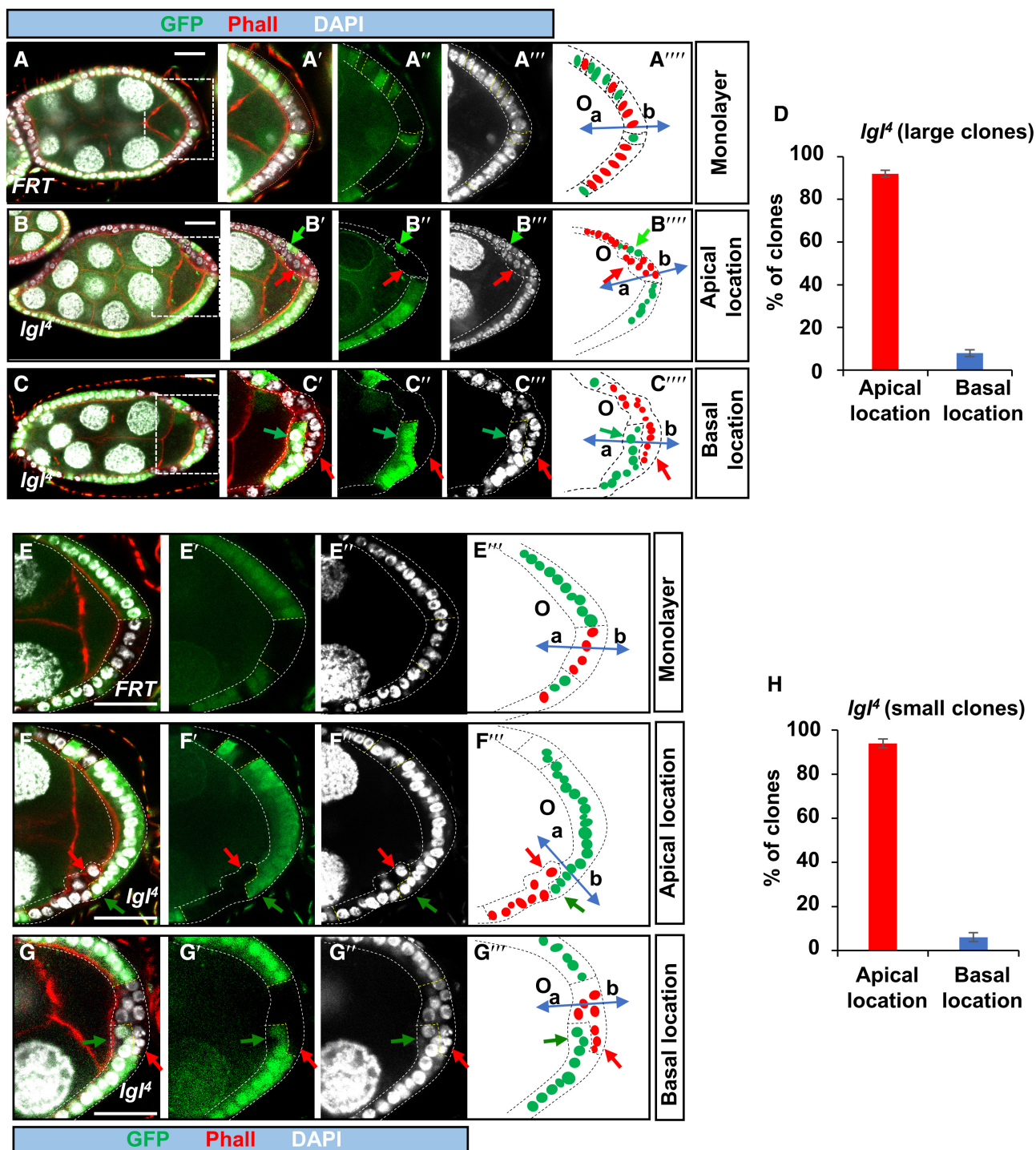


Figure 1.

We further examined the mosaic egg chambers bearing *aPKC* (*aPKC^{k06403}*) or *Baz* (*Baz^{Xi106}*) PFC clones. *Baz* and *aPKC* are components of the Par complex that regulate apical membrane identity. Contrary to *Igl* and *Dlg*, mosaic egg chambers carrying large *aPKC* or *Baz* PFC clones showed a preponderance of basal expansion of mutant cells (*aPKC^{k06403}*: 80%, $n = 81$, Figs 2C and EV3I-I' vs. K-K'; *Baz^{Xi106}*, 85%, $n = 78$, Figs 2E and EV3H-H' compared with Fig EV3J-J'). Small PFC clones revealed more clearly that the *aPKC*

and *Baz* mutant cells showed a strong preference to accumulate at the basal side of the nearby wildtype cells (*aPKC^{k06403}*: 83.2%, $n = 105$, Figs 2D and EV3E-E' vs. G-G', *Baz^{Xi106}*, 86.7%, $n = 123$, Figs 2F and EV3D-D' compared with Fig EV3F-F'). Additionally, the Z-stack analysis showed that the mutant cells of *Baz* were basally located (Fig EV3A and A', GFP⁻, red arrows) and showed clear connection with wildtype neighbors (Fig EV3B-C', green arrows). Further analysis of expression of PH3 in *Baz* mutant clones showed that

mutant cells can continue to divide after stage 7 (Fig 2I-I''' and J). Therefore, *aPKC* or *Baz* mutant cells show basal growth and form multilayers at the basal side of wildtype neighbors.

Taken together, these observations indicate that FCs with loss of polarity genes from different complexes can form distinct multi-layering patterns in the FE.

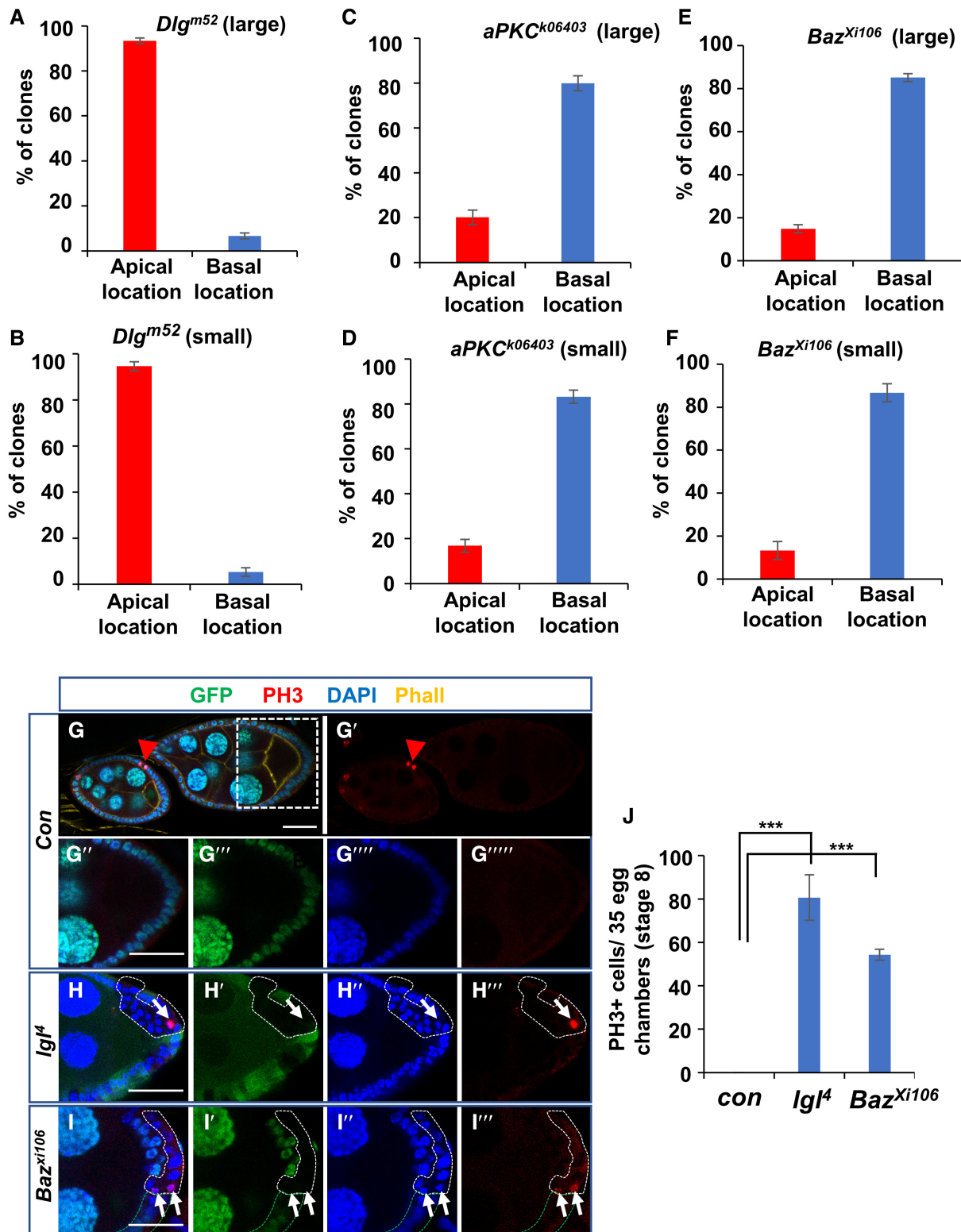


Figure 2.

Figure 2. The quantification of each location pattern in clones with loss of cell polarity genes.

- A The frequency of each location pattern in large clones was quantified for *Dlg*^{m52} (*n* = 75).
 B The frequency of each location pattern in small clones was quantified for *Dlg*^{m52} (*n* = 81).
 C The frequency of each location pattern in large clones was quantified for *aPKC* (*n* = 81).
 D The frequency of each location pattern in small clones was quantified for *aPKC* (*n* = 105).
 E The frequency of each location pattern in large clones was quantified for *Baz* (*n* = 78).
 F The frequency of each location pattern in small clones was quantified for *Baz* (*n* = 123).
 G–G''' The mitotic cell cycle marker phosphor-Histone H3 (PH3) was detected in FCs before stage 7 (red arrowheads), but not afterward in the wildtype egg chambers.
 H–H''' PH3 was detected in *lgl*^Δ mutant clones after stage 7 (arrows).
 I–I''' PH3 was detected in *Baz* mutant clones after stage 7 (arrows).
 J The quantification of PH3-positive cells in control, *lgl*, and *Baz* mutant clones at stage 8.

Data information: Scale bars represent 20 μm.

Three independent experiments were performed (A–F, and J). Error bars are ±SEM. ****P* < 0.001 (Student's *t*-test).

Source data are available online for this figure.

Downregulation of EGFR signaling is necessary for *lgl/Dlg*-loss-induced apical growth

As EGFR signaling is activated in the PFCs to induce a PFC fate (Gonzalez-Reyes *et al*, 1995; Roth *et al*, 1995), we asked whether its activation is involved in the regulation of multilayering patterns of polarity-deficient cells. To this end, we examined the expression of *pointed (pnt)-lacZ*, an EGFR signaling readout (Morimoto *et al*, 1996), and found that it was significantly reduced in *lgl*^Δ PFC clones (Fig 3B–B'' vs. A–A'', red arrows, *n* = 67), indicating downregulation of EGFR signaling in *lgl* PFC clones. Additionally, downregulation of *pnt-lacZ* was rescued by overexpression of an active form of EGFR (*EGFR*^{A887T}) (Fig EV4B–B''' vs. A–A''', *n* = 25). Loss of EGFR signaling in PFCs alone was not, however, sufficient to induce multilayering as loss-of-function (LOF) of EGFR PFC clones generated with *EGFR*^{f2Δ} or *EGFR-RNAi* did not show an obvious defect in monolayered epithelial organization (Gonzalez-Reyes *et al*, 1995; Roth *et al*, 1995) (Fig EV5B–B': *EGFR*^{f2}, GFP⁻, 100%, *n* = 94; C–C': *EGFR-RNAi*, GFP⁺, 100%, *n* = 112, compared with Control (A–A': 100%, *n* = 65)). In addition, the EGFR signaling activity in *EGFR*^{f2} was confirmed by *pnt-lacZ* expression (Fig EV5E vs. D, *n* = 19).

To determine whether downregulation of EGFR signaling is necessary for apical growth of *lgl* mutant FCs, we re-activated EGFR signaling by mis-expressing a constitutively active form of EGFR (*EGFR*^{A887T}) in *lgl*^Δ PFC clones (referred as *lgl*^Δ-*EGFR*^{A887T} clones) using the mosaic analysis with a repressible cell marker (MARCM) technique (Lee & Luo, 1999). As a control, follicle cells with clonal overexpression of *EGFR*^{A887T} alone maintained a monolayered epithelia and showed no defect in the epithelial organization (GFP⁺, Fig 3C–C'', 100%, *n* = 65). In contrast, activating EGFR signaling in *lgl*^Δ PFC clones (namely, *lgl*^Δ-*EGFR*^{A887T}) suppressed the apical accumulation phenotype of *lgl*^Δ mutant cells (Fig 3D–D'''). Instead, the *lgl*^Δ-*EGFR*^{A887T} cells were found over the basal side of their wildtype neighbors (Fig 3E–E''' and F). These findings suggest that activated EGFR signaling promotes basal growth of polarity-deficient *lgl* mutant FCs.

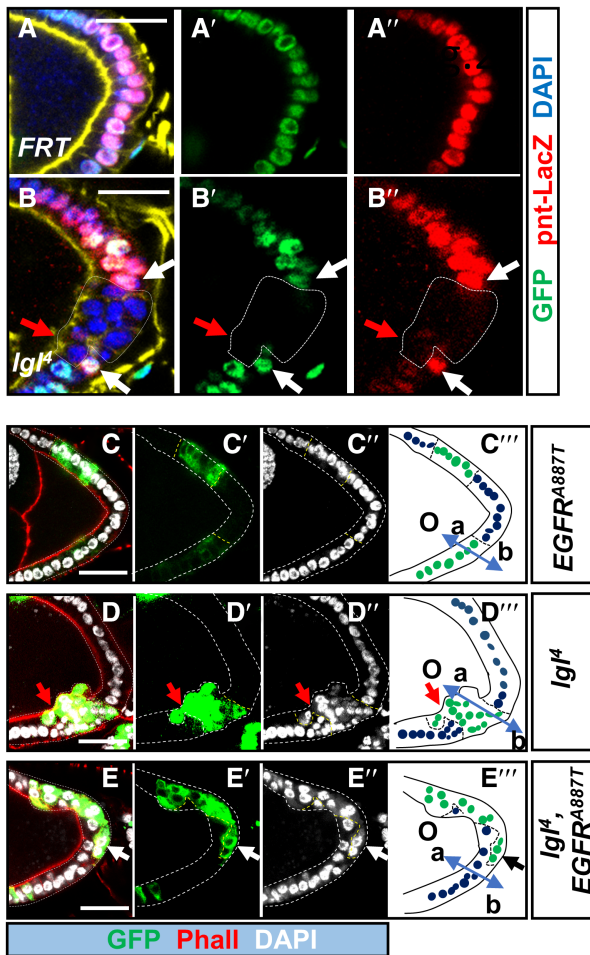
The EGFR activity promotes basal growth induced by loss of *aPKC/Baz* in the FE

To determine whether EGFR signaling is also involved in regulating basal expansion of the *aPKC* or *Baz* mutant cells, we examined expression of *pnt-lacZ* in *aPKC* mutant clones and found that its

expression remained high in *aPKC*^{k06403} mutant PFCs adjacent to the oocyte, suggesting that EGFR signaling is likely intact in these cells (Fig 4A–A'', white arrows). In *aPKC* mutant cells that were located more basally and did not maintain contact with the oocyte, *pnt-lacZ* appeared to be either diminished or lost (Fig 4A–A'', yellow arrowheads), probably because the oocyte-expressed ligand Grk (Gonzalez-Reyes *et al*, 1995; Roth *et al*, 1995) could no longer reach them.

When EGFR was knocked down with *UAS-EGFR-RNAi* in *aPKC* PFC clones (namely, *aPKC-EGFR*^{RNAi}) by means of the MARCM system, the frequency of basal expansion of polarity-deficient cells was markedly reduced (50% in *aPKC-EGFR*^{RNAi}, *n* = 60 vs. 80.1% in *aPKC*, *n* = 60), whereas the frequency of apical accumulation was dramatically increased (50% in *aPKC-EGFR*^{RNAi}, *n* = 60 vs. 19.9% in *aPKC*; *n* = 60) (Figs 4D–D'' vs. B–B'' and G). In contrast, the control FE with loss of EGFR signaling alone did not show apical or basal multilayering (Fig 4C–C'''). These results are consistent with the observations in *lgl* mosaic FE that EGFR signaling promotes basal growth of polarity-deficient FCs. Furthermore, upregulating EGFR signaling by expressing *EGFR*^{A887T}, which did not cause multilayering by itself (Fig 4E–E'''), in *aPKC* (named as *aPKC-EGFR*^{A887T}) PFC clones resulted in an enhanced multilayering phenotype with greater number of mutant cells accumulating at the basal side of adjacent wildtype cells (Fig 4F–F'', white arrows, Fig 4F''', black arrows), and increased percentage of PFC clones with basal buildup (94.5% in *aPKC-EGFR*^{A887T} vs. 80.1% in *aPKC*, *n* = 60 in each genotype; Fig 4F–F''' vs. B–B'' and H). Moreover, we found that activating EGFR signaling in *aPKC*^{k06403} FC clones located at the middle section of the egg chamber, where EGFR signaling is not activated and multilayers do not normally form, resulted in multilayers in 88% clones (*n* = 95) with basal expansion of mutant cells (Fig 4K, yellow arrows, compared with Fig 4I with *EGFR*^{A887T} expression and Fig 4J with *aPKC* clones at the middle section (white arrows), Fig 4L), further suggesting that EGFR signaling promotes basal expansion of polarity-deficient cells in the FE.

The effect of EGFR signaling on *lgl* and *aPKC* FCs prompted us to examine the relationship between *lgl/Dlg* and *aPKC/Baz* complexes in regulating formation of the multilayering patterns. To this end, we performed genetic epistatic analysis with the MARCM system and quantified the frequency of apical or basal growth of *lgl*^Δ PFCs with or without *aPKC* knockdown, and of *aPKC*^{k06403} PFCs with or without *lgl* knockdown. The results revealed that *lgl* knockdown in *aPKC*^{k06403} PFC clones substantially reduced the frequency of basal



F ■ Basal growth ■ Apical growth

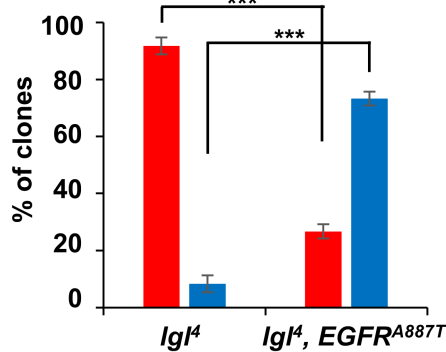


Figure 3.

growth (Appendix Fig S2, 55% in *aPKC^{k06403}* with *lgl-RNAi* vs. 80.1% in *aPKC^{k06403}*, $n = 60$ in each genotype). In contrast, *aPKC* knockdown in *lgl⁴* PFC clones did not change the frequency of apical growth (91.2% in *lgl⁴* with *aPKC-RNAi*, $n = 85$ vs. 92% in *lgl⁴* alone, $n = 75$), thereby indicating that *lgl* is epistatic to *aPKC* in regulating the multilayering patterns. This epistatic relationship is consistent with the different levels of EGFR signaling found in *lgl* and *aPKC* mutant PFCs, i.e., EGFR activity is absent in *lgl* but present in some *aPKC* mutant PFCs, and EGFR signaling promotes basal expansion of polarity-deficient cells.

Figure 3. Downregulation of EGFR signaling is required for apical accumulation.

A–B'' The EGFR signaling reporter *pnt-lacZ*, which was highly expressed in PFCs (A–A''), was significantly reduced in *lgl⁴* mutant PFCs (GFP⁺; B–B'', red arrows), whereas neighboring wildtype cells showed normal expression (white arrows).
 C–C'' The MARCM PFC clones (GFP⁺) with *UAS-EGFR^{A887T}* expression showed the monolayer.
 D–E'' Apical accumulation that was induced in *lgl⁴* MARCM PFC clones (GFP⁺) (D–D'') was suppressed by activated EGFR signaling with *UAS-EGFR^{A887T}* to form basal expansion (E–E'', white arrows, E'', black arrow).
 F The frequency of apical accumulation or basal expansion was quantified for indicated genotypes ($n = 64$).

Data information: The relative location between GFP⁺ cells (green) and GFP[−] cells (red) are illustrated in C'', D'' and E''. a: apical side; b: basal side; O: oocyte. Phallo: Phalloidin. Scale bars represent 20 μ m.

Three independent experiments were performed (F). Error bars are \pm SEM. *** $P < 0.001$ (Student's *t*-test).

Source data are available online for this figure.

scRNA-seq analysis identified cell clusters enriched with *Rok* expression

To determine how EGFR signaling regulates the growth direction, we performed single-cell RNA sequencing (scRNA-seq) analysis on ovaries bearing MARCM clones of *aPKC^{k06403}* with *EGFR^{A887T}* overexpression (*aPKC-EGFR^{A887T}*) and the wildtype control. To compare cell populations that were present in the wildtype and *aPKC-EGFR^{A887T}* datasets, the two datasets were merged into an integrated dataset, which was ultimately divided into 42 clusters (Fig 5A). Based on the expression of *GFP*, *Act5C*, and *EGFR* (Fig 5B–G), 11 clusters from *aPKC-EGFR^{A887T}* mutant cells were identified (clusters 14, 15, 33, 34, 35, 37, 38, 39, 40, 41, and 42; Fig 5A, red arrows and green arrows). Among these clusters, six (clusters 37, 38, 39, 40, 41, and 42) were identified as specific clusters containing only *aPKC-EGFR^{A887T}* cells (red arrows in Fig 5A). In addition, all 36 clusters except for the six specific ones were annotated on the basis of expression of marker genes (Fig 5A and Appendix Fig S3) identified from the previous scRNA-seq analysis of the wildtype egg chamber (Jevitt et al, 2020).

Among the *aPKC-EGFR^{A887T}*-specific clusters, clusters 38 and 39 showed enrichment of genes such as *Rho kinase (Rok)* (Fig 5I, blue arrows, compared with Fig 5H), *pointed (pnt)*, a downstream gene of EGFR signaling), *cappuccino (capu)*, *Rho1*, *mysospheroid (mys)*, and *inflated (if)*. *Rok*, which phosphorylates Spaghetti squash (Sqh), the regulatory myosin light chain (RMLC) of nonmuscle myosin II in *Drosophila* (Edwards & Kiehart, 1996; Wang & Riechmann, 2007), is involved in the remodeling of actin/actomyosin cytoskeleton and regulation of cell extrusion/delamination (Fernandez et al, 2007; Cram, 2014). Our further qRT-PCR analysis with *aPKC-RNAi* knockdown in FCs confirmed that *Rok* expression was upregulated (Fig 5J). In addition, we examined *Rok* expression in *lgl* mutant cells with *lgl-RNAi* and found that *Rok* expression was downregulated (Fig 5J).

The *Rok* kinase activity can be detected by an antibody against phospho-specific RMLC (pRMLC), and the level of pRMLC was used as the readout for the *Rok* activity (Wang & Riechmann, 2007). In wildtype follicle cells, pRMLC is enriched at the apical cortex (Fig 6A–A'', $n = 35$), which was confirmed by *sqh* mutant clones

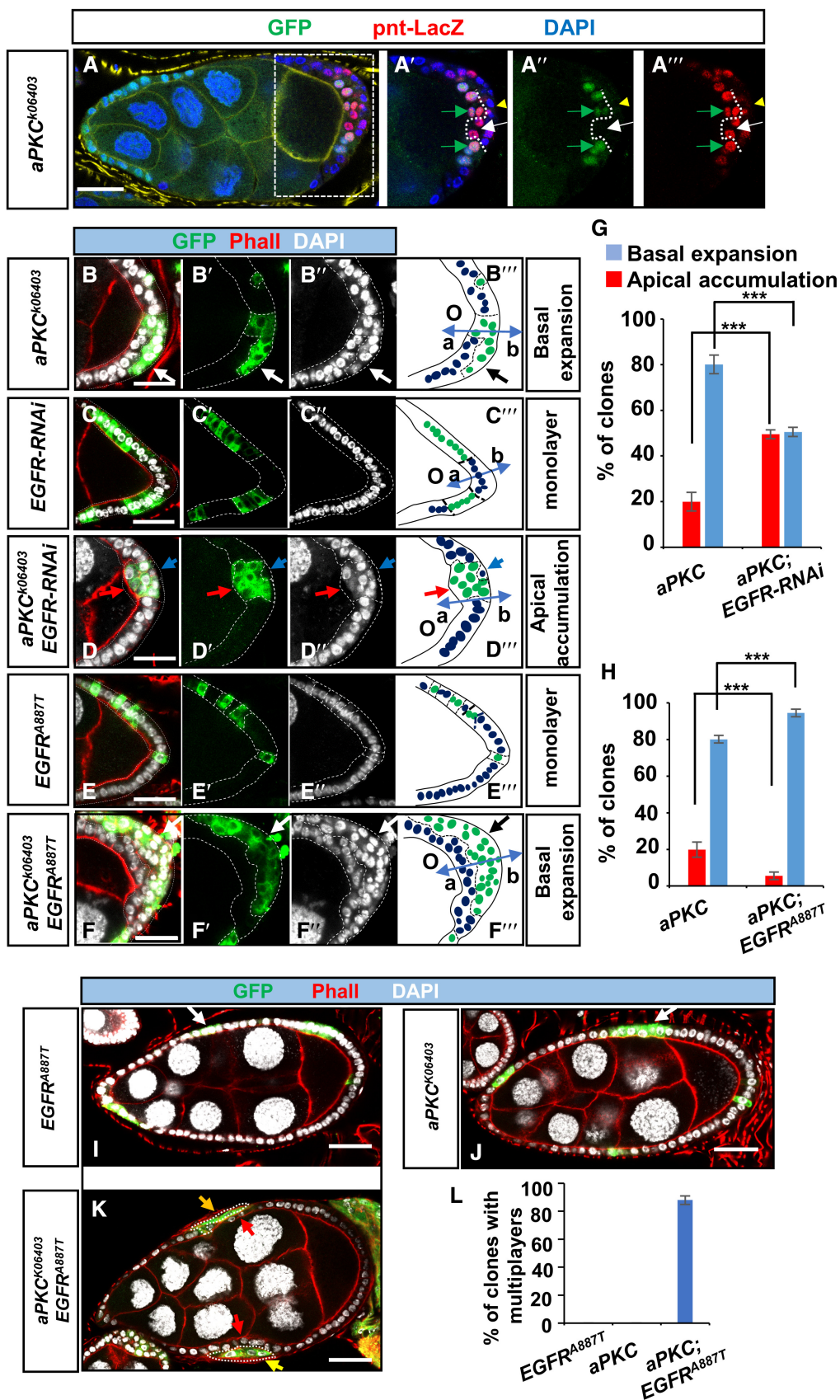


Figure 4.

Figure 4. Basal expansion of *aPKC* mutant FCs is regulated by EGFR signaling.

- A–A'' The EGFR signaling reporter *pnt-lacZ* remained highly expressed in *aPKC*^{k06403} mutant cells (white arrow) and in neighboring wildtype cells (green arrows) but was downregulated once these cells (yellow arrowhead) lost contact with the oocyte.
- B–B'' *aPKC* MARCM PFC clones (GFP⁺) showed basal expansion (white arrows).
- C–C'' The MARCM PFC clones (GFP⁺) with *UAS-EGFR-RNAi* expression showed the monolayer.
- D–D'' The expression of *UAS-EGFR-RNAi* in *aPKC*^{k06403} cells (GFP⁺) switched basal expansion in *aPKC*^{k06403} PFC clones to apical expansion (red arrows). The blue arrows show the neighboring wildtype cells.
- E–E'' The MARCM PFC clones (GFP⁺) with *UAS-EGFR*^{A887T} expression showed the monolayer.
- F–F'' *UAS-EGFR*^{A887T} expression (GFP⁺) in *aPKC*^{k06403} PFC clones enhanced basal expansion (white arrows, black arrow in F'').
- G, H The frequency of apical accumulation or basal expansion was quantified for indicated genotypes, *n* = 60 for each genotype. Error bars are ±SEM. ****P* < 0.001.
- I Activation of EGFR signaling with *UAS-EGFR*^{A887T} at the lateral region (white arrow) did not induce multilayers.
- J *aPKC*^{k06403} mutant cells did not induce basal expansion and multilayers at the lateral region (white arrow).
- K Activation of EGFR signaling with *UAS-EGFR*^{A887T} in *aPKC*^{k06403} FC clones induced the multilayered phenotype and produced basal expansion at the lateral regions (yellow arrows). The red arrows show the wildtype neighbors.
- L The frequency of clones with multilayers at the lateral region of egg chambers, *n* = 95 for each genotype.

Data information: a: apical side; b: basal side; O: oocyte. Phall: Phalloidin. Scale bars represent 20 μm.

Three independent experiments were performed (G, H, L). Error bars are ±SEM. ****P* < 0.001 (Student's *t*-test).

Source data are available online for this figure.

(Appendix Fig S4). To determine whether EGFR signaling regulates Rok activity in follicle cells, we examined the level of pRMLC in *aPKC* mutant cells. We found that the intensity of the pRMLC in *aPKC* mutant cells is comparable to that in wildtype cells (Fig 6B–B'' and I). However, pRMLC in *aPKC* mutant cells was distributed through the entire cortex (Fig 6B–B'', *n* = 40). Moreover, when *EGFR*^{A887T} was expressed in *aPKC* mutant cells, we observed a significant upregulation of the pRMLC level in the entire cortex (Fig 6C–C'', *n* = 35 clones, Fig 6I). These results suggest that activation of EGFR signaling upregulates the pRMLC level. In support of this conclusion, we found that the pRMLC level was reduced in *lgl* mutant cells where EGFR activity was decreased (Fig 6D–D'', *n* = 40, Fig 6J). This decrease of pRMLC was rescued by *EGFR*^{A887T} overexpression in *lgl* mutant cells (Fig 6E–E'', *n* = 38, Fig 6J). In addition, we examined the level of pRMLC when *EGFR*^{A887T} or *EGFR-RNAi* was expressed in follicle cells and found that pRMLC was upregulated by *EGFR*^{A887T} (Fig 6F–F'', *n* = 34, Fig 6K), but downregulated by *EGFR-RNAi* expression (Fig 6G–G'', *n* = 31, Fig 6K). As a control, expression of the dominant-negative *Rok* in FCs can reduce pRMLC level (Fig 6H–H'', *n* = 17, Fig 6K). Together, these results suggest that Rok and Sqh/RLMC are critical targets of EGFR signaling in FCs.

Rok and RMLC (*sqh*) regulate the direction of multilayer formation in FE

To determine whether different levels of pRMLC in *lgl* and *aPKC* mutant cells control apical or basal growth of FCs with loss of polarity genes, we lowered the pRMLC level in *aPKC* mutant cells by overexpressing a dominant-negative and kinase-dead form of *Rok* (*Rok*^{DN}) or a nonphosphorylatable form of *sqh* (*sqh*^{CA}). As expected, overexpression of either *UAS-Rok*^{DN} or *UAS-sqh*^{CA} in *aPKC*^{k06403} PFC clones reduced the frequency of basal growth (86.7% in *aPKC*^{k06403} vs. 63.9% in *aPKC*^{k06403}-*Rok*^{DN}, and 67.2% in *aPKC*^{k06403}-*sqh*^{CA}; *n* = 60 in each genotype) and increased the frequency of apical growth (13.3% in *aPKC*^{k06403} vs. 36.1% in *aPKC*^{k06403}-*Rok*^{DN}, and 32.8% in *aPKC*^{k06403}-*sqh*^{CA}; *n* = 60 in each genotype) (Fig 7A–C'' and D). Additionally, overexpression of *UAS-Rok*^{DN} suppressed the basal growth of *aPKC* mutant cells with *EGFR*^{A887T} expression (Fig 7L and K–K'' vs. I–J'', *n* = 35). As the control, overexpression of *UAS-Rok*^{DN} or *UAS-*

sqh^{DN} in follicle cells with MARCM did not induce the multilayering phenotypes (Appendix Fig S5B and D). Therefore, downregulation of Rok-Sqh activity promotes a switch from basal to apical growth of polarity-deficient FCs.

Furthermore, we enhanced Rok-Sqh activity by expressing a constitutively active form of *Rok* (*Rok*^{CA}) or a phosphomimetic form of *sqh* (*sqh*^{CA}) in *lgl*⁴ PFC clones, and found that expression of either *Rok*^{CA} or *sqh*^{CA} in *lgl*⁴ PFC clones alleviated the apical growth phenotype with less frequency (93.3% in *lgl*⁴ vs. 42% in *lgl*⁴-*Rok*^{CA}, and 47.2% in *lgl*⁴-*sqh*^{CA}; *n* = 60 in each genotype) and increased the frequency of basal growth (6.7% in *lgl*⁴ vs. 58% in *lgl*⁴-*Rok*^{CA}, and 52.8% in *lgl*⁴-*sqh*^{CA}; *n* = 60 in each genotype) (Fig 7E–G'' and H). In control egg chambers, overexpression of *UAS-Rok*^{CA} and *UAS-sqh*^{CA} in FCs with MARCM did not induce multilayering (Appendix Fig S5A and C). These findings suggest that upregulation of Rok-Sqh activity promotes basal growth.

Together, these genetic epistasis analyses indicate that *Rok* and *Sqh* phosphorylation is critical in the FE to regulate the direction of accumulation of polarity-deficient cells.

Rok acts as a downstream target of the EGFR-Pnt pathway

EGFR signaling in the FCs is mediated by a downstream transcription factor Pnt (Morimoto *et al*, 1996). The study with chromatin immunoprecipitation sequencing (ChIP-seq) in the *Drosophila* intestine showed that the enhancer of *Rok* was a binding target of Pnt (Zhang *et al*, 2022). Thus, we wondered if *Rok* is transcriptionally regulated by Pnt in the FE. To test this possibility, we analyzed the promoter region of *Rok* using JASPAR (Sandelin *et al*, 2004) and identified three potential Pnt-binding sites (Fig 8A). Using an anti-GFP antibody to perform a ChIP analysis with Pnt-GFP expressing ovary, the three potential Pnt target segments (Amplicons 1, 2, and 3) were selected for the qPCR analysis and the result showed that Pnt strongly bound to two sites (sites 1 and 3) and weakly bound to one site (site 2) (Fig 8B and C). Furthermore, a qRT-PCR analysis with ovaries containing *Pnt* overexpressing FCs showed that *Rok* expression was upregulated (Fig 8D). Together, these studies indicate that *Rok* is a transcriptional target of Pnt in the FE.

To corroborate that Pnt mediates the role of EGFR signaling in regulating apical or basal growth of polarity-deficient PFCs, *pnt* was

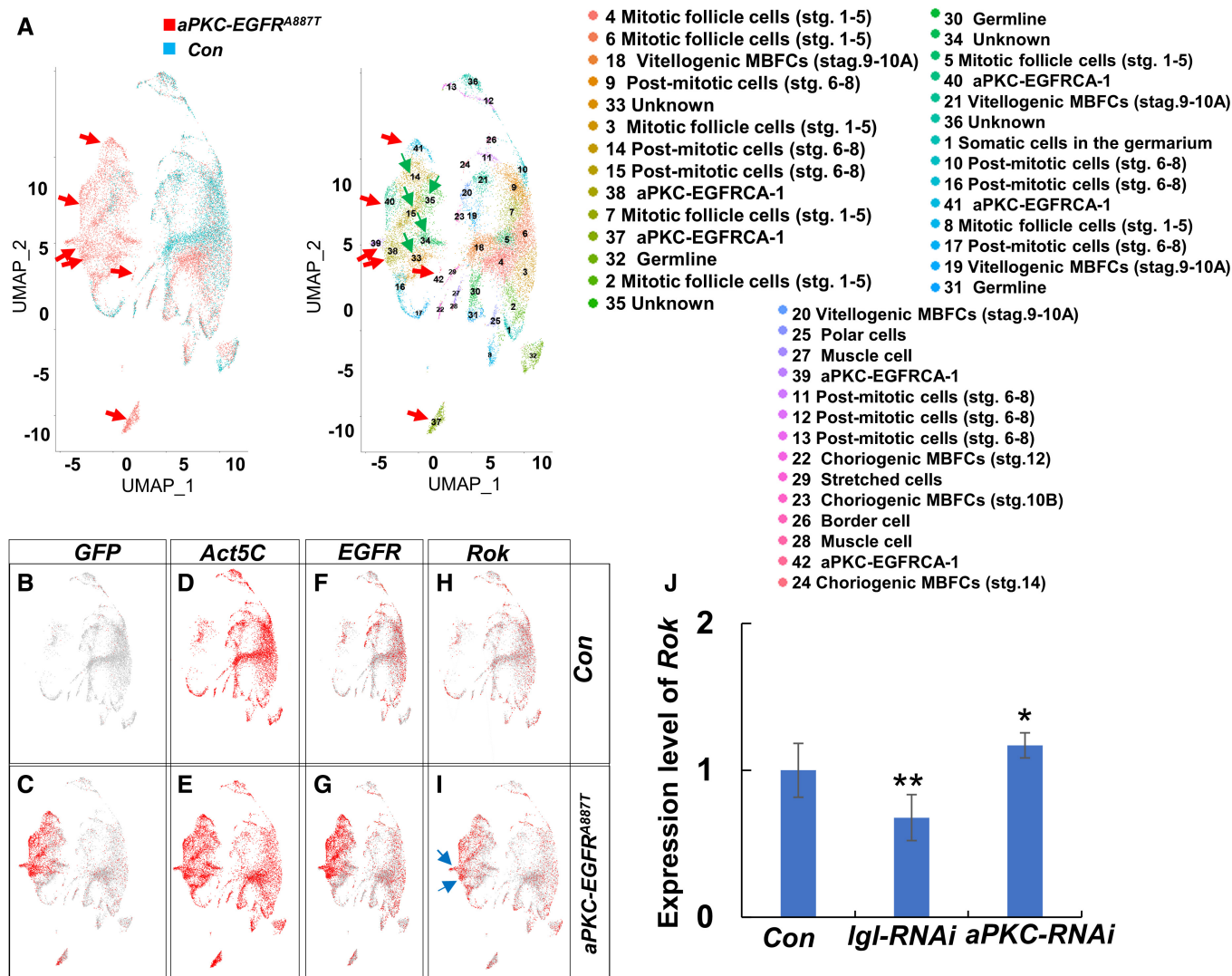


Figure 5. Upregulation of *Rok* expression in aPKC-EGFR^{A887T} clones was identified by scRNA-seq analysis.

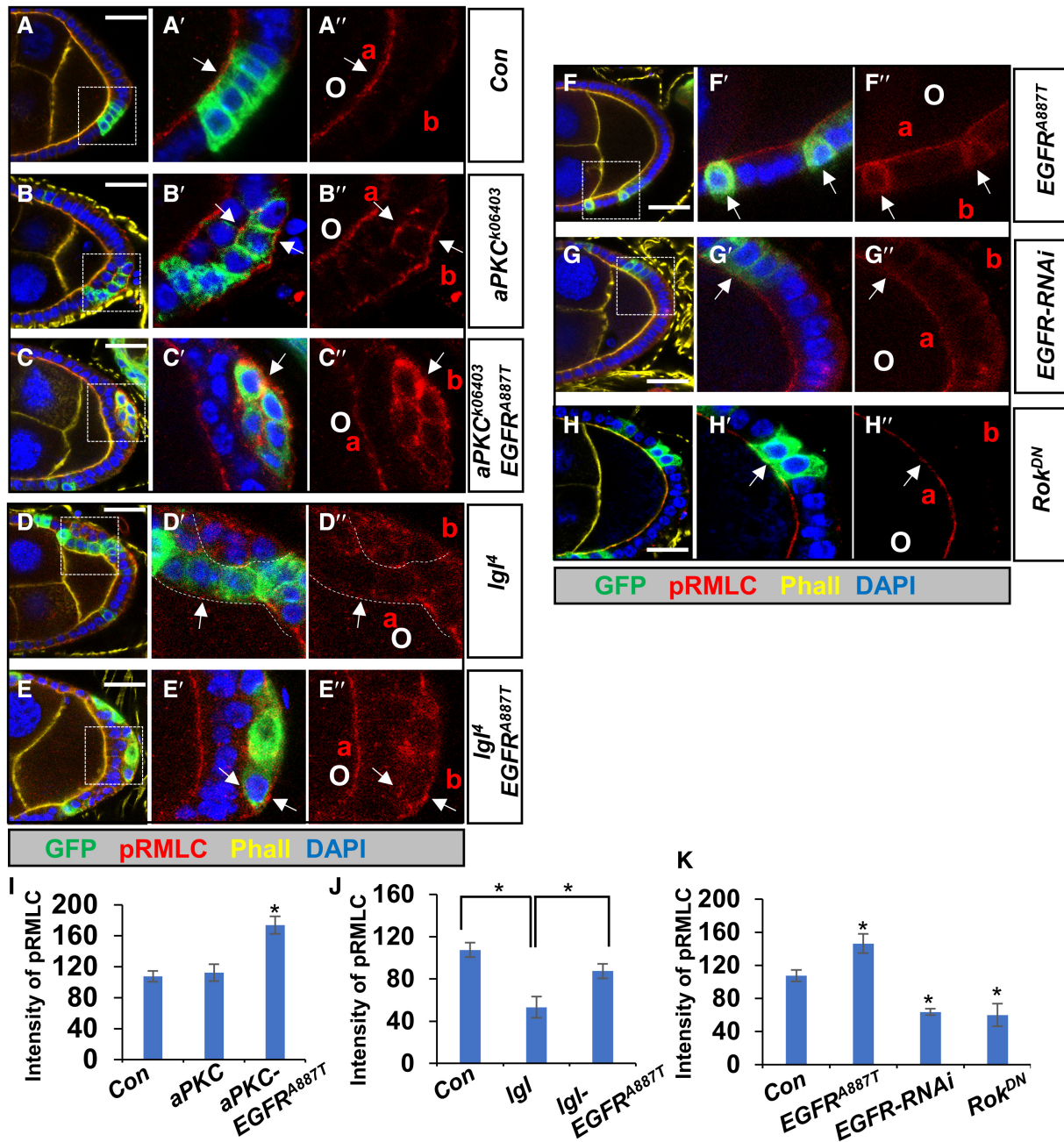
A High-quality cells from wildtype (Con) and aPKC-EGFR^{A887T} were grouped into 42 clusters, which were labeled according to the expression of marker genes.
 B, C According to expression of GFP, aPKC-EGFR^{A887T} mutant clones were identified in A (red arrows and green arrowheads). The red arrows indicate the specific clusters for aPKC-EGFR^{A887T} cells.
 D, E The expression of *Act5C* was used as the control.
 F, G *EGFR* expression in each cluster was shown.
 H, I Cells in clusters 38 and 39 (blue arrows) show enriched expression of *Rok* (I, blue arrows, compared with H in the wildtype).
 J *Rok* expression was measured by qRT-PCR in wildtype, *lgl* knockdown, and aPKC knockdown FCs ($n = 3$).

Data information: Three independent experiments were performed (J). Error bars are \pm SEM. ** $P < 0.01$, and * $P < 0.05$ (Student's *t*-test). Source data are available online for this figure.

overexpressed in *lgl* mutant FCs using the MARCM technique. These mosaic FE showed that the growth direction of *lgl* PFCs was switched from a predominantly apical to a basal preference (Fig 8E, 93.6% in *lgl*^Δ vs. 31% in *lgl*^Δ-*Pnt*; $n = 67$). This phenotype is similar to *lgl* PFC clones with re-activated EGFR signaling (Fig 3E-E''), suggesting that *Pnt* acts downstream of EGFR signaling to regulate the growth direction of polarity-deficient FCs. Taken together, these findings connect EGFR signaling and the actomyosin cytoskeletal regulators *Rok*-*Sqh* through transcription factor *Pnt* in the control of polarity loss-induced multilayering.

Discussion

Intact epithelial cell polarity maintains the integrity and protects cells from unnecessary growth, extrusion or invasion. The direction through which they escape the epithelial layer has a profound impact on their fates, which include cell death and overgrowth (Tamori et al, 2016). In this study, using the *Drosophila* FE model, we found that EGFR signaling was differentially regulated in the PFCs with loss of *lgl/Dlg* or *Baz/aPKC*, and demonstrated that different levels of EGFR signaling activity in PFCs controlled the direction



of formation of multilayers when apical-basal polarity was disrupted (Fig 9B and C, compared with Fig 9A). Using scRNA-seq analysis, we identified enrichment of *Rok* expression in mutant cells with simultaneous *aPKC* loss and EGFR activation. Further studies with qRT-PCR and ChIP analyses suggest that *Rok* is a transcriptional

target of *Pnt*, which is downstream of EGFR signaling (Gabay et al, 1996). *Rok*, through the control of phosphorylation of RMLC, modulates the actomyosin network and epithelial organization. pRMLC is enhanced in mutant cells with basal accumulation where EGFR signaling is intact. Upregulation of EGFR signaling in these

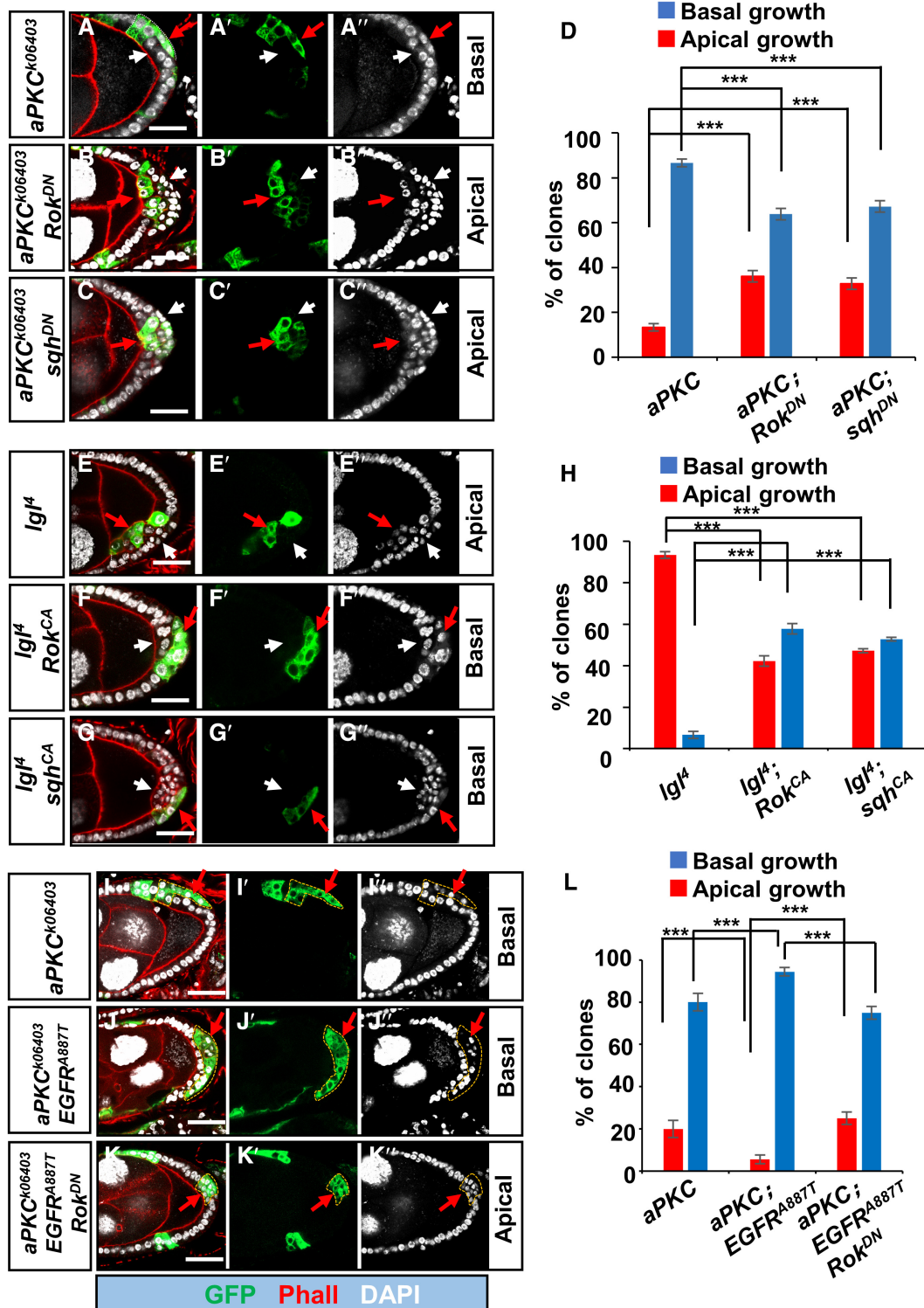


Figure 7. Directional growth is regulated by the Rok-Sqh axis.

A–A'' Loss of *aPKC*-induced basal growth (red arrows).
 B–C'' Overexpression of *Rok^{DN}* (B–B'') or *sqh^{DN}* (C–C'') in *aPKC* mutant PFCs induced apical growth (red arrows). White arrows indicated the wildtype neighbors.
 E–E'' *Igl* mutant cells showed apical growth (red arrows). White arrows indicated the wildtype neighbors.
 F–G'' Overexpression of *Rok^{CA}* (F–F'') or *sqh^{CA}* (G–G'') in *Igl⁴* PFC clones switched apical growth to basal growth (red arrows). White arrows indicated the wildtype neighbors.
 I–I'' Loss of *aPKC*-induced basal growth (red arrows).
 J–J'' Expression of *EGFR^{887T}* enhances basal growth (red arrows).
 K–K'' Expression of *Rok^{DN}* repressed basal growth in *aPKC* mutant clones with *EGFR^{887T}* (red arrows).
 D, H, L The frequency of apical growth or basal growth was quantified for indicated genotypes ($n = 60$). Scale bars represent 20 μm .
 Data information: Three independent experiments were performed (D, H, L). Error bars are \pm SEM. *** $P < 0.001$ (Student's *t*-test).
 Source data are available online for this figure.

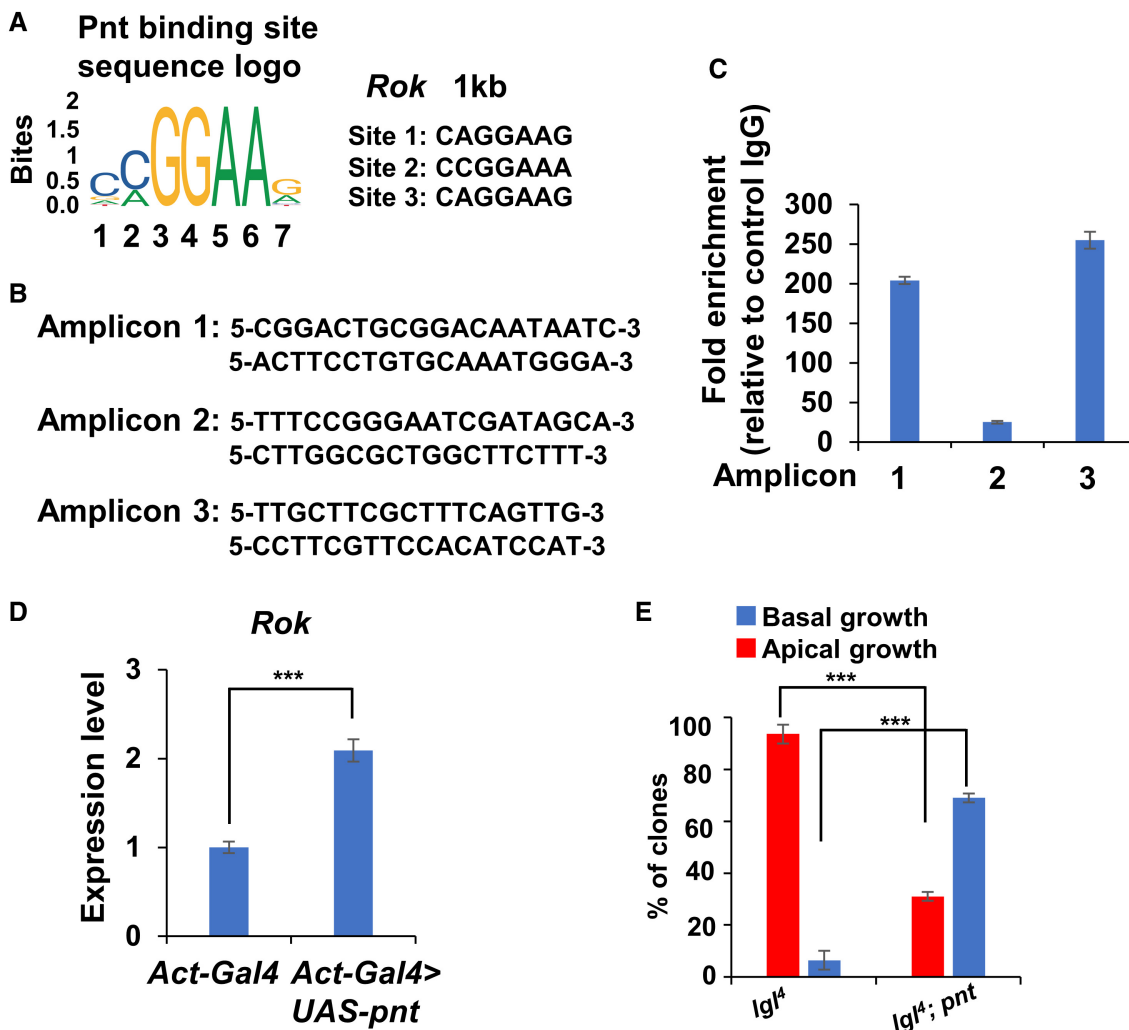


Figure 8. Rok acts as a transcriptional target of Pnt.

A The consensus Pnt-binding sites and three consensus Pnt-binding sequences were found in 1 kb promoter/enhancer region of *Rok*.
 B, C The ChIP experiment detects direct binding of Pnt-GFP to the promoter/enhancer region of *Rok*. Transgenic flies with pnt-GFP were subject to ChIP experiment using the anti-GFP antibody. The enhancer regions detected by different primers for sites 1, 2, and 3 were shown in B.
 D The qRT-PCR shows that overexpression of Pnt in follicle cells upregulated *Rok* expression.
 E The frequency of apical growth or basal growth was quantified for indicated genotypes, $n = 60$ for each genotype.

Data information: Three independent experiments were performed (D, E). Error bars are \pm SEM. *** $P < 0.001$ (Student's *t*-test).
 Source data are available online for this figure.

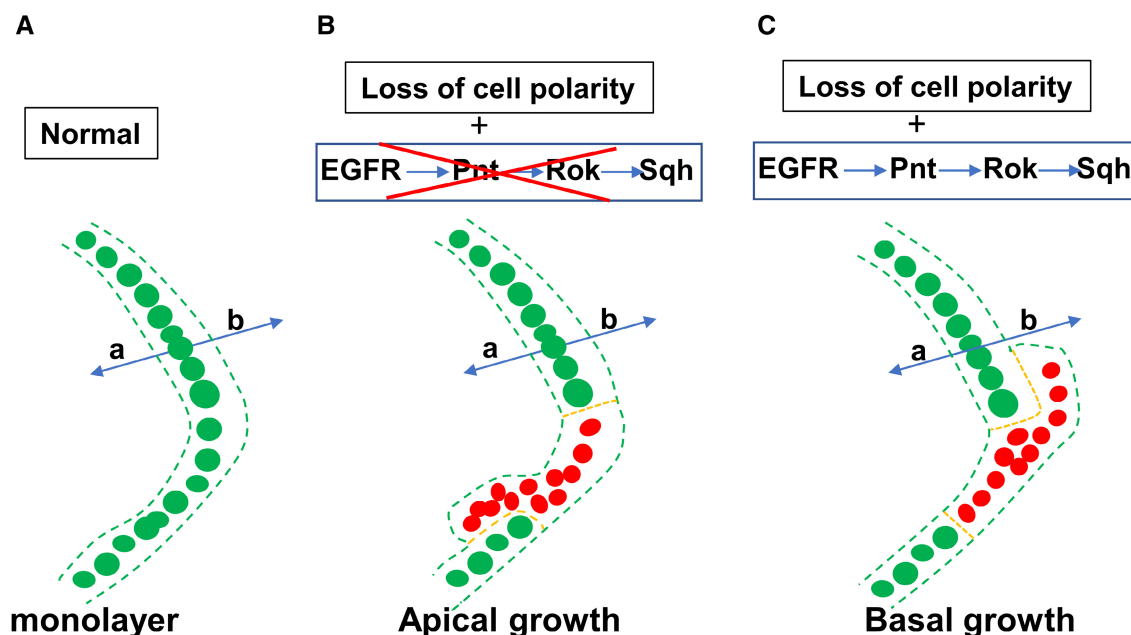


Figure 9. A model for the regulation of apical and basal growth in polarity-deficient cells by EGFR signaling and the Rok-Sqh regulatory axis.

A The wildtype follicle cells show a monolayer.

B, C In follicle cells with polarity loss, reduction of EGFR signaling downregulates the Rok-Sqh signal to promote apical growth (B), but EGFR signaling upregulates Rok-Sqh signal to induce basal growth (C).

cells resulted in further accumulation of pRMLC around the cell cortex. These findings thereby suggest an EGFR-Pnt-Rok-RMLC regulatory axis that governs the pattern of epithelial overgrowth upon polarity loss.

Epithelial cells experiencing a loss of polarity can exit the epithelial layer through extrusion or delamination processes (Slattum & Rosenblatt, 2014). The mechanisms governing directional extrusion/delamination involve the disruption of intercellular junctions and the contraction of actomyosin (Rosenblatt *et al*, 2001; Slattum *et al*, 2009; Gu *et al*, 2011; Tamori *et al*, 2016; Ohsawa *et al*, 2018). Typically, cortical actomyosin first contracts apically within the extruding cell, while actomyosin cables in surrounding cells collaborate to squeeze out the extruding cell (Rosenblatt *et al*, 2001; Zulueta-Coarasa & Rosenblatt, 2021). In the FE model, polarity-deficient cells were not observed to undergo apoptosis, and they maintained connections with wildtype cells, forming multilayers alongside their neighboring wildtype cells. The specific regulatory factors governing the directional localization, whether it involves contraction or cell shape changes, remain to be investigated.

Our studies have found that EGFR signaling is differentially regulated in FCs when various cell polarity complexes are lost, but the underlying mechanism remains elusive. The fate of EGFR protein, either being sorted to lysosomes for degradation or the plasma membrane for recycling (Madshus & Stang, 2009; Tomas *et al*, 2014) (Ceresa, 2006; Rappoport & Simon, 2009) (Nishimura & Itoh, 2019), plays a fundamental role in regulating EGFR signaling. The distinctions in EGFR signaling regulation by the Lgl/Dlg/Scrb and Par complexes might be due to their specific molecular functions. The Scrib complex, for example, is involved in retromer-dependent sorting events that facilitate the return of internalized

cargo to the cell surface (de Vreede *et al*, 2014) (Stephens *et al*, 2018), which could affect the recycling of the EGFR protein. On the other hand, the Par complex has been found to act downstream of Cdc42 to regulate the apical endocytotic pathway (Harris & Tepass, 2008), which may not significantly impact EGFR membrane trafficking. Hence, the regulation of EGFR signaling by these cell polarity complexes could involve their influence on EGFR localization at the plasma membrane or their impact on EGFR degradation processes. As a result, further investigation into how different cell polarity complexes affect the trafficking of the EGFR protein and its subsequent impact on EGFR signaling is intriguing and should be pursued in future studies. This may shed light on the intricate molecular mechanisms underlying EGFR regulation and its connections to cell polarity pathways.

During oogenesis, multiple signaling pathways are activated to specify the fates of anterior follicle cells (AFCs) and PFCs. Without EGFR signaling, the PFC may adopt an AFC-like behavior, which includes the invasion by border cells that migrate through the germline nurse cells. The unmasking of EGFR signaling by *lgl/Dlg* mutations may allow the mutant PFC behave like invasive border cells, which still depend on Jak-STAT signaling for their migration. This may explain why lateral follicle cells and early follicle cells do not normally invade inwards upon polarity loss. The complexity of the AFCs also includes the activation of PDGF signaling, another RTK signaling that may be needed for apical growth prevention. Therefore, it would be interesting to determine whether the AFCs undergo directional growth upon polarity loss and what the underlying mechanisms are.

In studies, the *Drosophila* wing imaginal disc epithelia (Appendix Fig S6A–A'') have been used as a model system to investigate cell

delamination and invasion. Specifically, we examined the localization of *lgl* and *aPKC* mutant cells in comparison with neighboring wildtype cells in the notum regions. Interestingly, we observed that *lgl* mutant cells tended to be localized at the apical side of wildtype neighboring cells (Appendix Fig S6B–B''', 89%, $n = 23$). On the other hand, *aPKC* mutant cells were found to accumulate at the basal side of neighboring cells (Appendix Fig S6C–C''', 91%, $n = 32$). These observations indicate that the location patterns of these mutant cells closely resemble those observed in FCs, highlighting the conserved phenotype in the different tissues. However, whether the EGFR signaling pathway is involved in regulation of this process in the wing discs will be explored in our future studies.

Clinically, tumors from pancreatic ducts, retina, kidney, and tongue of mammals show exophytic and endophytic growth, which is defined by tumor cells growing out of or crawling under the epithelium (Harasymczuk et al, 2013). The apical and basal location of mutant cells revealed in the *Drosophila* FE model resembles the endophytic and exophytic growth of tumor in humans, respectively. Clinical studies revealed that exophytic tumor growth is associated with a high level of EGFR expression (Phuc et al, 2021), and the increased expression of EGFR has also been identified in a variety of cancers to promote tumor growth (Sharma et al, 2007; Sasaki et al, 2013). Our studies indicate that activation of EGFR signaling is associated with basal growth direction and upregulation of EGFR signaling can further enhance their basal expansion, suggesting that the regulatory mechanism learned in the *Drosophila* FE model could be applied to cancer studies. In addition, the studies in the mouse found that the tension imbalance and tissue curvature in tubular epithelia regulate different tumor growth patterns (Messal et al, 2019). As endophytic or exophytic tumors have different prognosis and postoperative local recurrence (Kirita et al, 1994; Tsivian et al, 2010; Eslami et al, 2015), these models from *Drosophila* and mammals provide platforms for identifying intrinsic signaling pathways, biophysical parameters, and microenvironment involved in the regulation of these different growth pattern tumors.

Materials and Methods

Fly strains and clone generation.

The strains we used were raised at 25°C on standard media. The following flies were used: *lgl*⁴ *FRT40A/Cyo* (strong LOF allele), *lgl*^{27S3} *FRT40A/Cyo* (LOF allele), *FRT42D apk*^{k06403}/*Cyo* (strong LOF allele), *Baz*^{Xi106}*FRT9-2*, *Dlg*^{m30}*FRT19A*, and *Dlg*^{m52}*FRT19A*. Transgenic lines: *UAS-EGFR-RNAi* (VDRC43267), *UAS-EGFR*^{A887T} (BL#9536), *UAS-aPKC-RNAi* (BL#25946), *UAS-lgl-RNAi* (VDRC51249), *pointed-LacZ* (*pnt-LacZ*), *UAS-Rok*^{DN} (kinase dead, BL#6671), *UAS-sqh*^{DN} (nonphosphorylatable sqh, BL#64114), *UAS-Rok*^{CA} (active form of Rok, BL#6669), *UAS-sqh*^{CA} (phospho-mimic, BL#64411), *sqh*^{AX3}*FRT19A/FM7c* (BL#25712), *hsFlp*, *act > CD2 > Gal4*, *UAS-RFP*, *Pnt-GFP* (BL#42680). Follicular mosaic clones and MARCM clones were generated by FLP-FRT-induced mitotic recombination (Xu & Rubin, 1993), and the following strains were used: *ywhsFLP*; *Ubi-GFPFRT40A/Cyo*, *ywhsFLP*; *FRT42D Ubi-GFPFP/Cyo*, *Ubi-hGFP FRT9-2/FM7c*; *hsFlp/TM6*, *hsFlp RFP FRT19A*, *hsFLP*; *FRT42D tubGAL80/cyo*; *actin-GAL4 UAS-mCD8:GFP*, *hsFLP*; *tubGAL80 FRT40A*; *actin-GAL4 UAS-mCD8:GFP*. For generation of

mosaic clones and MARCM clones, adult flies with the appropriate genotypes were subjected to heat shock at 37°C for 1 h, and flies were raised at 25°C for different periods before dissection. To ensure consistency and avoid spatio-temporal discrepancies in phenotypes, we examined posterior follicle cells (PFCs) in stage 7–10 egg chambers with 5–7 days of incubation time after clone induction (ACI).

Immunohistochemistry

Ovaries were dissected out and fixed in 4% paraformaldehyde solution, and the following primary antibodies were applied according to standard antibody staining procedures (Tian & Deng, 2008): rabbit anti-galactosidase, 1:2000 (Sigma); goat anti-GFP (Abcam, Cambridge, MA); Rabbit anti-pRMLC, 1:100 (Cell Signaling); and Alexa Fluor 633 Phalloidin and 488 Phalloidin, 1:50 (Invitrogen). Secondary antibodies conjugated to Alexa Fluor 546 donkey anti-mouse and anti-rabbit (Molecular Probes) and Alexa Fluor 633 donkey anti-mouse and anti-rabbit and 488 Donkey anti-goat (Jackson immunoresearch) were used at 1:400. Fluorescently labeled samples were counterstained with DAPI for visualization of DNA. Images were captured with a Zeiss LSM 800 confocal microscope and assembled in Adobe Photoshop.

scRNA-seq sample preparation, sequencing, and data analysis

Drosophila ovaries with the desired genotypes (*hsFLP*; *FRT42D tubGAL80/FRT42DaPKC*^{k06403}; *actin-GAL4 UAS-mCD8:GFP/UAS-EGFR*^{A887T} and *hsFLP*; *FRT40A tubGAL80/FRT40A*; *actin-GAL4 UAS-mCD8:GFP*) at 6-d ACI were then dissected in complete medium (Grace's Insect Basal Medium supplemented with 15% fetal bovine serum) as previously described (Jevitt et al, 2020). To prevent cell clumping, ovaries were transferred to a tube containing 300 µl Earle's Balanced Salt Solution (EBSS) (no calcium, magnesium, and phenol red) and gently washed for 2 min. The EBSS was then removed, and the tissue was dissociated in 100 µl Papain (50 U/ml in EBSS and previously heat activated in 37°C for 15 min) for 30 min. The suspension was mechanically dissociated every 3 min by gentle pipetting up and down. To quench the digestion, 500 µl complete medium was added to dissociated cells. The suspension was then passed through a 40 µl sterile cell strainer and centrifuged for 10 min at 700 RCF to remove debris and large eggs with intact eggshells that could not be dissociated. This process also filtered out larger germline cells, which increase dramatically in size around stage 9 (Kolahi et al, 2009). The supernatant was removed, and single cells were resuspended in 100 µl. Cell viability was assayed with AOPI solution, and cell number was determined with a Nexcelom Cellometer. Cells were then further diluted to an approximate, final density of 2,000 cells/µl according to 10× Genomics. Libraries were generated by Chromium Next GEM Single Cell v3.1 and were sequenced in a NovaSeq 6000 (Illumina) at Florida State University. Cell Ranger (version 3.0.0) processing resulted in a total of 307,977,702 reads with mean 39,945 reads per cell for wildtype (con), and 234,288,861 reads with mean 21,245 reads per cell for *aPKC-EGFR*^{A887T}. Seurat (Butler et al, 2018; Stuart et al, 2019) was used for log-normalization and scaling of the data by means of default parameters and was used to integrate the two datasets from the wildtype and *aPKC-EGFR*^{A887T} into a single dataset, and RunUMAP with a resolution of 2 was used to group the integrated dataset.

Chromatin immunoprecipitation coupled with qPCR

Approximately 50 pairs of ovaries were used in each experiment, dissected from females raised at 25°C on standard cornmeal/agar medium. Samples are prepared as previously described (Evolutionarily Conserved Roles for Apontic in Induction and subsequent Decline of Cyclin E Expression). Briefly, dissected ovaries were fixed with 1% formaldehyde for 20 min at room temperature. After fixation, samples were terminated with 2.5 M glycine, homogenized with lysis buffer, and stored at -80°C until needed. Samples were sonicated with the Covaris M220 130- μ l microtube using the setting of Peak Incident Power 50, Duty Factor 20%, Cycle per Burst 200, and Treatment Time 150 s. An average size of 150–200 bp was produced. The resulting chromatin was processed in three ways. First, 5% of the chromatin was heat treated to reverse cross-links and phenol-chloroform extracted to generate the input DNA fraction. Second, the remaining chromatin was divided into two fractions. One fraction was incubated with anti-GFP antibody (2 μ l) (abcam-ab290) and the other with control Rabbit IgG (2 μ l). Enriched DNA was obtained by incubation with protein A beads (Sigma 16-661) and phenol-chloroform extraction.

RT-qPCR

Total RNAs were prepared from approximately 10 pairs of ovaries using Rneasy Plus Mini Kit (Zymo Research, Cat. number R2050). cDNA was synthesized using the iScript cDNA synthesis kit (Bio-Rad). RT-qPCR was performed using iQ SYBR Green System (Bio-Rad). *RpL11* was used as a normalization control. Primers for *Rok*: 5'-TACGAATGCAAGAGATGC-3' and 5'-CGGGTCGTGTTGTCCACAT-3'. Relative quantification of mRNA levels was calculated using the comparative CT method. Statistical analyses were performed by Student's *t*-test.

Statistical analyses

Statistical analyses were performed with a two-tailed unpaired *t*-test. *P*-value is indicated by asterisks in the Figures: ***P* < 0.01; ****P* < 0.001. Differences at *P* < 0.01 were considered significant.

Genotypes for flies in each figure

Figure 1. (A–A''', E–E'') *ywhsFLP*; *Ubi-GFP**FRT40A/FRT40A*. (B–B''', C–C''', F–F'', G–G'') *ywhsFLP*; *Ubi-GFP**FRT40A/lgl⁴FRT40A*.

Figure 2. (A, B) *hsFLP* *Ubi-RFP* *FRT19A/Dlg^{m52}FRT19A*. (C, D) *ywhsFLP*; *FRT42DUbi-GFP**FRT42DaPKC^{k06403}*. (E, F) *Baz^{Xi106}FRT9-2/Ubi-His2A-GFP**FRT9-2*; *hsFlp/+*. (G–G''') *ywhsFLP*; *Ubi-GFP**FRT40A/FRT40A*. (H–H''') *ywhsFLP*; *Ubi-GFP**FRT40A/lgl⁴FRT40A*. (I–I''') *Baz^{Xi106}FRT9-2/Ubi-His2A-GFP**FRT9-2*; *hsFlp/+*.

Figure 3. (A–A'') *ywhsFLP*; *Ubi-GFP**FRT40A/FRT40A*; *pnt-LacZ/+*. (B–B'') *ywhsFLP*; *Ubi-GFP**FRT40A/lgl⁴FRT40A*; *pnt-LacZ/+*. (C–C'') *hsFLP*; *tubGAL80* *FRT40A/FRT40A*; *actin-GAL4* *UAS-GFP/UAS-EGFR^{A887T}*. (D–D'') *hsFLP*; *tubGAL80* *FRT40A/lgl⁴FRT40A*; *actin-GAL4* *UAS-mCD8:GFP*. (E–E'') *hsFLP*; *tubGAL80* *FRT40A/lgl⁴FRT40A*; *actin-GAL4* *UAS-mCD8:GFP/UAS-EGFR^{A887T}*.

Figure 4 (A–A''') *ywhsFLP*; *FRT42DUbi-GFP**FRT42D aPKC^{k06403}*; *pnt-LacZ*. (B–B'', J) *hsFLP*; *FRT42D* *tubGAL80/FRT42DaPKC^{k06403}*; *actin-GAL4* *UAS-mCD8:GFP*. (C–C'') *hsFLP*; *FRT42D* *tubGAL80/*

FRT42D; *actin-GAL4* *UAS-mCD8:GFP/UAS-EGFR-RNAi*. (D–D'') *hsFLP*; *FRT42D* *tubGAL80/FRT42DaPKC^{k06403}*; *actin-GAL4* *UAS-mCD8:GFP/UAS-EGFR-RNAi*. (E–E'', I) *hsFLP*; *FRT42D* *tubGAL80/FRT42D*; *actin-GAL4* *UAS-mCD8:GFP/UAS-EGFR^{A887T}*. (F–F'', K) *hsFLP*; *FRT42D* *tubGAL80/FRT42DaPKC^{k06403}*; *actin-GAL4* *UAS-mCD8:GFP/UAS-EGFR^{A887T}*.

Figure 6. (A–A'') *hsFLP*; *FRT42D* *tubGAL80/FRT42D*; *actin-GAL4* *UAS-mCD8:GFP*. (B–B'') *hsFLP*; *FRT42D* *tubGAL80/FRT42DaPKC^{k06403}*; *actin-GAL4* *UAS-mCD8:GFP*. (C–C'') *hsFLP*; *FRT42D* *tubGAL80/FRT42DaPKC^{k06403}*; *actin-GAL4* *UAS-mCD8:GFP/UAS-EGFR^{A887T}*. (D–D'') *hsFLP*; *tubGAL80* *FRT40A/lgl⁴FRT40A*; *actin-GAL4* *UAS-mCD8:GFP*. (E–E'') *hsFLP*; *tubGAL80* *FRT40A/lgl⁴FRT40A*; *actin-GAL4* *UAS-mCD8:GFP/UAS-EGFR^{A887T}*. (F–F'') *hsFLP*; *tubGAL80* *FRT40A/FRT40A*; *actin-GAL4* *UAS-mCD8:GFP/UAS-EGFR^{A887T}*. (G–G'') *hsFLP*; *tubGAL80* *FRT40A/FRT40A*; *actin-GAL4* *UAS-mCD8:GFP/UAS-EGFR-RNAi*. (H–H'') *hsFLP*; *tubGAL80* *FRT40A/FRT40A*; *actin-GAL4* *UAS-mCD8:GFP/UAS-Rok^{DN}*.

Figure 7. (A–A'') *hsFLP*; *FRT42D* *tubGAL80/FRT42DaPKC^{k06403}*; *actin-GAL4* *UAS-mCD8:GFP/+*. (B–B'') *hsFLP*; *FRT42D* *tubGAL80/FRT42DaPKC^{k06403}*; *actin-GAL4* *UAS-mCD8:GFP/UAS-Rok^{DN}*. (C–C'') *hsFLP*; *FRT42D* *tubGAL80/FRT42DaPKC^{k06403}*; *actin-GAL4* *UAS-mCD8:GFP/UAS-sqh^{DN}*. (E–E'') *hsFLP*; *tubGAL80* *FRT40A/lgl⁴FRT40A*; *actin-GAL4* *UAS-mCD8:GFP*. (F–F'') *hsFLP*; *tubGAL80* *FRT40A/lgl⁴FRT40A*; *actin-GAL4* *UAS-mCD8:GFP/UAS-Rok^{CA}*. (G–G'') *hsFLP*; *tubGAL80* *FRT40A/lgl⁴FRT40A*; *actin-GAL4* *UAS-mCD8:GFP/UAS-sqh^{CA}*. (I–I'') *hsFLP*; *FRT42D* *tubGAL80/FRT42DaPKC^{k06403}*; *actin-GAL4* *UAS-mCD8:GFP/+*. (J–J'') *hsFLP*; *FRT42D* *tubGAL80/FRT42DaPKC^{k06403}*; *actin-GAL4* *UAS-mCD8:GFP/EGFR^{A887T}*. (K–K'') *hsFLP*; *FRT42D* *tubGAL80/FRT42DaPKC^{k06403}*; *actin-GAL4* *UAS-mCD8:GFP/EGFR^{A887T}* *Rok^{DN}*.

Genotypes for flies in each supplementary figure

Figure EV1. (A–C') *ywhsFLP*; *Ubi-GFP**FRT40A/lgl⁴FRT40A*. (D–G'') *hsFLP* *Ubi-RFP* *FRT19A/Dlg^{m52}FRT19A*.

Figure EV2. (A–B) *ywhsFLP*; *Ubi-GFP**FRT40A/lgl²⁷⁵³FRT40A*. (C–D) *hsFLP* *Ubi-RFP* *FRT19A/Dlg^{m30}FRT19A*.

Figure EV3. (A–C', D–D'', F–F'', H–H'', J–J'') *Baz^{Xi106}FRT9-2/Ubi-His2A-GFP**FRT9-2*; *hsFlp/+*. (E–E'', G–G'', I–I'', K–K'') *ywhsFLP*; *FRT42DUbi-GFP**FRT42DaPKC^{k06403}*.

Figure EV4. (A–A'') *hsFLP*; *tubGAL80* *FRT40A/lgl⁴FRT40A*; *actin-GAL4* *UAS-mCD8:GFP/pnt-lacZ*. (B–B'') *hsFLP*; *tubGAL80* *FRT40A/lgl⁴FRT40A*; *actin-GAL4* *UAS-mCD8:GFP/EGFR^{A887T}* *pnt-lacZ*.

Figure EV5. (A–A') *ywhsFLP*; *Ubi-GFP**FRT40A/FRT40A*. (B–B'') *ywhsFLP*; *Ubi-GFP**FRT40A/EGFR^{F24}FRT40A*. (C–C'') *hsFLP*; *tubGAL80* *FRT40A/FRT40A*; *actin-GAL4* *UAS-mCD8:GFP/EGFR-RNAi*. (D–D'') *ywhsFLP*; *Ubi-GFP**FRT40A/FRT40A*; *pnt-lacZ/+*. (E–E'') *ywhsFLP*; *Ubi-GFP**FRT40A/EGFR^{F24}FRT40A*; *pnt-lacZ/+*.

Data availability

All raw sequence files are available from the SRA repository: SRR26353200 and SRR26353201 (<http://www.ebi.ac.uk/ena/data/view/SRR26353200> and <http://www.ebi.ac.uk/ena/data/view/SRR26353201>).

Expanded View for this article is available online.

Acknowledgements

We thank Dr. David Bilder, Bloomington *Drosophila* Stock Center for stocks (NIH P400D018537), and Developmental Studies Hybridoma Bank for providing fly lines and antibodies. We also thank Drs. Hong Liu and Jun-yuan Ji for careful reading of the manuscript and Kejing Song from Tulane University, Yanming Yang, and Cynthia Vied from Florida State University for single-cell library preparation and sequencing. This work was supported by the National Institutes of Health P20GM103629, A Carol Lavin Bernick Faculty Grant, Bridge Research Fund at Tulane University and Bridge Research Fund at SOM to AT, and the National Institutes of Health GM072562, CA224381, and CA227789 to WMD.

Author contributions

Aiguo Tian: Conceptualization; formal analysis; funding acquisition; investigation; methodology; writing – original draft; project administration; writing – review and editing. **Xian-Feng Wang:** Formal analysis; investigation. **Yuting Xu:** Data curation; investigation. **Virginia Morejon:** Data curation; investigation. **Yi-Chun Huang:** Data curation; investigation. **Chidi Nwupuda:** Formal analysis. **Wu-Min Deng:** Conceptualization; funding acquisition; writing – review and editing.

Disclosure and competing interests statement

The authors declare that they have no conflict of interest.

References

- Abdelilah-Seyfried S, Cox DN, Jan YN (2003) Bazooka is a permissive factor for the invasive behavior of discs large tumor cells in *Drosophila* ovarian follicular epithelia. *Development* 130: 1927–1935
- Antel M, Inaba M (2020) Modulation of cell-cell interactions in *Drosophila* oocyte development. *Cell* 9: 274
- Bastock R, St Johnston D (2008) *Drosophila* oogenesis. *Curr Biol* 18: R1082–R1087
- Bilder D (2004) Epithelial polarity and proliferation control: links from the *Drosophila* neoplastic tumor suppressors. *Genes Dev* 18: 1909–1925
- Bilder D, Li M, Perrimon N (2000) Cooperative regulation of cell polarity and growth by *Drosophila* tumor suppressors. *Science* 289: 113–116
- Bilder D, Schober M, Perrimon N (2003) Integrated activity of PDZ protein complexes regulates epithelial polarity. *Nat Cell Biol* 5: 53–58
- Butler A, Hoffman P, Smibert P, Papalexis E, Satija R (2018) Integrating single-cell transcriptomic data across different conditions, technologies, and species. *Nat Biotechnol* 36: 411–420
- Ceresa BP (2006) Regulation of EGFR endocytic trafficking by rab proteins. *Histol Histopathol* 21: 987–993
- Chatterjee D, Costa CAM, Wang XF, Jevitt A, Huang YC, Deng WM (2022) Single-cell transcriptomics identifies Keap1-Nrf2 regulated collective invasion in a *Drosophila* tumor model. *Elife* 11: e80956
- Coradini D, Casarsa C, Oriana S (2011) Epithelial cell polarity and tumorigenesis: new perspectives for cancer detection and treatment. *Acta Pharmacol Sin* 32: 552–564
- Cram EJ (2014) Mechanotransduction in *C. elegans* morphogenesis and tissue function. *Prog Mol Biol Transl Sci* 126: 281–316
- Deng WM, Althausen C, Ruohola-Baker H (2001) Notch-Delta signaling induces a transition from mitotic cell cycle to endocycle in *Drosophila* follicle cells. *Development* 128: 4737–4746
- Edwards KA, Kiehart DP (1996) *Drosophila* nonmuscle myosin II has multiple essential roles in imaginal disc and egg chamber morphogenesis. *Development* 122: 1499–1511
- Eslami A, Miyaguchi K, Mogushi K, Watanabe H, Okada N, Shibuya H, Mizushima H, Miura M, Tanaka H (2015) PARVB overexpression increases cell migration capability and defines high risk for endophytic growth and metastasis in tongue squamous cell carcinoma. *Br J Cancer* 112: 338–344
- Fernandez BG, Arias AM, Jacinto A (2007) Dpp signalling orchestrates dorsal closure by regulating cell shape changes both in the amnioserosa and in the epidermis. *Mech Dev* 124: 884–897
- Gabay L, Scholz H, Golembo M, Klaes A, Shilo BZ, Klambt C (1996) EGF receptor signaling induces pointed P1 transcription and inactivates Yan protein in the *Drosophila* embryonic ventral ectoderm. *Development* 122: 3355–3362
- Gonzalez-Reyes A, Elliott H, St Johnston D (1995) Polarization of both major body axes in *Drosophila* by gurken-torpedo signalling. *Nature* 375: 654–658
- Goode S, Perrimon N (1997) Inhibition of patterned cell shape change and cell invasion by Discs large during *Drosophila* oogenesis. *Genes Dev* 11: 2532–2544
- Gu Y, Forostyan T, Sabbadini R, Rosenblatt J (2011) Epithelial cell extrusion requires the sphingosine-1-phosphate receptor 2 pathway. *J Cell Biol* 193: 667–676
- Harasymczuk M, Gooding W, Kruk-Zagajewska A, Wojtowicz J, Dworacki G, Tomczak H, Szyfter W, Whiteside TL (2013) Head and neck squamous carcinomas with exophytic and endophytic type of growth have the same prognosis after surgery and adjuvant radiotherapy. *Eur Arch Otorhinolaryngol* 270: 1105–1114
- Harris KP, Tepass U (2008) Cdc42 and Par proteins stabilize dynamic adherens junctions in the *Drosophila* neuroectoderm through regulation of apical endocytosis. *J Cell Biol* 183: 1129–1143
- Hong Y, Stronach B, Perrimon N, Jan LY, Jan YN (2001) *Drosophila* stardust interacts with crumbs to control polarity of epithelia but not neuroblasts. *Nature* 414: 634–638
- Jevitt A, Chatterjee D, Xie G, Wang XF, Otwell T, Huang YC, Deng WM (2020) A single-cell atlas of adult *Drosophila* ovary identifies transcriptional programs and somatic cell lineage regulating oogenesis. *PLoS Biol* 18: e3000538
- Jevitt A, Huang YC, Zhang SM, Chatterjee D, Wang XF, Xie GQ, Deng WM (2021) Modeling notch-induced tumor cell survival in the *Drosophila* ovary identifies cellular and transcriptional response to nuclear NICD accumulation. *Cells* 10: 2222
- Kirita T, Okabe S, Izumo T, Sugimura M (1994) Risk factors for the postoperative local recurrence of tongue carcinoma. *J Oral Maxillofac Surg* 52: 149–154
- Kolahi KS, White PF, Shreter DM, Classen AK, Bilder D, Mofrad MR (2009) Quantitative analysis of epithelial morphogenesis in *Drosophila* oogenesis: New insights based on morphometric analysis and mechanical modeling. *Dev Biol* 331: 129–139
- Lee T, Luo L (1999) Mosaic analysis with a repressible cell marker for studies of gene function in neuronal morphogenesis. *Neuron* 22: 451–461
- Li Q, Feng S, Yu L, Zhao G, Li M (2011) Requirements of Lgl in cell differentiation and motility during *Drosophila* ovarian follicular epithelium morphogenesis. *Fly (Austin)* 5: 81–87
- Lopez-Schier H, St Johnston D (2001) Delta signaling from the germ line controls the proliferation and differentiation of the somatic follicle cells during *Drosophila* oogenesis. *Genes Dev* 15: 1393–1405
- Madhus IH, Stang E (2009) Internalization and intracellular sorting of the EGF receptor: a model for understanding the mechanisms of receptor trafficking. *J Cell Sci* 122: 3433–3439
- Messal HA, Alt S, Ferreira RMM, Gribben C, Wang VM, Cotoi CG, Salbreux G, Behrens A (2019) Tissue curvature and apicobasal mechanical tension imbalance instruct cancer morphogenesis. *Nature* 566: 126–130

- Morimoto AM, Jordan KC, Tietze K, Britton JS, O'Neill EM, Ruohola-Baker H (1996) Pointed, an ETS domain transcription factor, negatively regulates the EGF receptor pathway in *Drosophila* oogenesis. *Development* 122: 3745–3754
- Nanavati BN, Yap AS, Teo JL (2020) Symmetry breaking and epithelial cell extrusion. *Cell* 9: 1416
- Nishimura Y, Itoh K (2019) Involvement of SNX1 in regulating EGFR endocytosis in a gefitinib-resistant NSCLC cell lines. *Cancer Drug Resist* 2: 539–549
- Ohsawa S, Vaughen J, Igaki T (2018) Cell extrusion: a stress-responsive force for good or evil in epithelial homeostasis. *Dev Cell* 44: 284–296
- Phuc ND, Ky LM, Binh NT, Thuc VTM, Tuan NT, Van NTK, Hai TX (2021) Correlation of EGFR (Her1) expression with clinical features in sinonasal squamous cell carcinoma. *Genet Mol Res* 20: GMR18749
- Rappoport JZ, Simon SM (2009) Endocytic trafficking of activated EGFR is AP-2 dependent and occurs through preformed clathrin spots. *J Cell Sci* 122: 1301–1305
- Richardson HE, Portela M (2018) Modelling cooperative tumorigenesis in *Drosophila*. *Biomed Res Int* 2018: 4258387
- Rosenblatt J, Raff MC, Cramer LP (2001) An epithelial cell destined for apoptosis signals its neighbors to extrude it by an Actin- and myosin-dependent mechanism. *Curr Biol* 11: 1847–1857
- Roth S, Neuman-Silberberg FS, Barcelo G, Schupbach T (1995) Cornichon and the EGF receptor signaling process are necessary for both anterior-posterior and dorsal-ventral pattern formation in *Drosophila*. *Cell* 81: 967–978
- Royer C, Lu X (2011) Epithelial cell polarity: a major gatekeeper against cancer? *Cell Death Differ* 18: 1470–1477
- Sandelin A, Alkema W, Engstrom P, Wasserman WW, Lenhard B (2004) JASPAR: an open-access database for eukaryotic transcription factor binding profiles. *Nucleic Acids Res* 32: D91–D94
- Sasaki T, Hiroki K, Yamashita Y (2013) The role of epidermal growth factor receptor in cancer metastasis and microenvironment. *Biomed Res Int* 2013: 546318
- Shahab J, Tiwari MD, Honemann-Capito M, Krahn MP, Wodarz A (2015) Bazooka/PAR3 is dispensable for polarity in *Drosophila* follicular epithelial cells. *Biol Open* 4: 528–541
- Sharma SV, Bell DW, Settleman J, Haber DA (2007) Epidermal growth factor receptor mutations in lung cancer. *Nat Rev Cancer* 7: 169–181
- Slattum GM, Rosenblatt J (2014) Tumour cell invasion: an emerging role for basal epithelial cell extrusion. *Nat Rev Cancer* 14: 495–501
- Slattum G, McGee KM, Rosenblatt J (2009) P115 RhoGEF and microtubules decide the direction apoptotic cells extrude from an epithelium. *J Cell Biol* 186: 693–702
- Stephens R, Lim K, Portela M, Kvensakul M, Humbert PO, Richardson HE (2018) The scribble cell polarity module in the regulation of cell signaling in tissue development and tumorigenesis. *J Mol Biol* 430: 3585–3612
- Stuart T, Butler A, Hoffman P, Hafemeister C, Papalexi E, Mauck WM 3rd, Hao Y, Stoeckius M, Smibert P, Satija R (2019) Comprehensive integration of single-cell data. *Cell* 177: 1888–1902
- Tamori Y, Suzuki E, Deng WM (2016) Epithelial tumors originate in tumor hotspots, a tissue-intrinsic microenvironment. *PLoS Biol* 14: e1002537
- Tian AG, Deng WM (2008) Lgl and its phosphorylation by aPKC regulate oocyte polarity formation in *Drosophila*. *Development* 135: 463–471
- Tomas A, Futter CE, Eden ER (2014) EGF receptor trafficking: consequences for signaling and cancer. *Trends Cell Biol* 24: 26–34
- Tsvivan M, Lyne JC, Mayes JM, Mouraviev V, Kimura M, Polascik TJ (2010) Tumor size and endophytic growth pattern affect recurrence rates after laparoscopic renal cryoablation. *Urology* 75: 307–310
- de Vreede G, Schoenfeld JD, Windler SL, Morrison H, Lu H, Bilder D (2014) The Scribble module regulates retromer-dependent endocytic trafficking during epithelial polarization. *Development* 141: 2796–2802
- Wang Y, Riechmann V (2007) The role of the actomyosin cytoskeleton in coordination of tissue growth during *Drosophila* oogenesis. *Curr Biol* 17: 1349–1355
- Xu T, Rubin GM (1993) Analysis of genetic mosaics in developing and adult *Drosophila* tissues. *Development* 117: 1223–1237
- Zhang C, Jin Y, Marchetti M, Lewis MR, Hammouda OT, Edgar BA (2022) EGFR signaling activates intestinal stem cells by promoting mitochondrial biogenesis and beta-oxidation. *Curr Biol* 32: e3707
- Zulueta-Coarasa T, Rosenblatt J (2021) The role of tissue maturity and mechanical state in controlling cell extrusion. *Curr Opin Genet Dev* 72: 1–7



License: This is an open access article under the terms of the [Creative Commons Attribution-NonCommercial-NoDerivs](https://creativecommons.org/licenses/by-nc-nd/4.0/) License, which permits use and distribution in any medium, provided the original work is properly cited, the use is non-commercial and no modifications or adaptations are made.